Exp. Theo. NANOTECHNOLOGY 7 (2023) 41 - 54 https://doi.org/10.56053/7.1.41

Structural, electronic, and optoelectronic properties of XYZ_2 (X=Zn,Cd; Y=Si,Sn; Z=pnicogens) Chalcopyrite compounds: First-principles calculations

Oula Jabbar, Ali H. Reshak

Physics Department, College of Science, University of Basrah, Basrah 61004, Iraq
*) Email: oula.jabbar@yahoo.com

Received 13/5/2022, *Accepted*, 23/12//2022, *Published* 15/1/2023

Structural, optoelectronic and electronic characteristics of the semiconductor chalcopyrite XYZ_2 (X=Zn, Cd; Y=Si, Sn; Z=P) are predicted using first-principleS calculations. The (PBE-GGA) is used for the geometrical relaxation whereas the (TB-mBJ) potential is used to determine the ground state properties. The bandgap decreases by substituting Si by Sn in XYP_2. The calculated energy bandgap values exhibit good consistency with experimental evidence and prior theoretical findings. The d-states of Zn and Cd contribute greatly to the density of states in $XSiP_2$, Sn-d states are predominant in the $XSnP_2$. Given its great reflectivity in UV region makes XYP_2 good candidate for photonic and optoelectronic devices.

Keywords: Chalcopyrite; DFT; Electronic; Optoelectronic.

1. INTRODUCTION

Ternary compounds $A^{II}B^{IV}C_2^{V}$ and $A^{I}B^{III}C_2^{VI}$ having chalcopyrite structure, with space group $I\bar{4}2d$, due to their structural, mechanical, electronic, and nonlinear optical characteristics, are extremely useful [1]. By increasing the unit cell along the (c) z-axis in binary zinc-blende structures, the chalcopyrite structures are obtained from the analogs III-V and II-VI, giving rise to a tetragonal unit cell with its center in the body. According to the zinc-blende structure, each cation/anion is surrounded by its four closest neighbors' anions/cations. In a tetrahedral bonding of the two cation sublattice, the A and B cations take turns occupying the Zn-positions. When compared to their binary counterparts, the ternary compounds' band gap is substantially less due to the diminished symmetry [2]. They are extensively utilized in a variety of fields, including photovoltaic, optoelectronic, spintronic, non-linear optical, solar

energy converters, detectors, light-emitting diodes, and many more [3-12]. The direct-band gap of the compounds is between (0.2) and (2.2) eV, indicating that they exhibit semiconducting properties [13]. $ZnSnP_2$ is a material used as an absorber in solar cells, and its band gap may be successfully tuned by adjusting the cation disorder [14]. The band gap is direct and it is valued at approximately 1.0 eV for $ZnSiP_2$. [15]. Due to its low parasitic below-band gap absorption, $ZnSiP_2$ is a potential material for solar cells, super photo response, and high open circuit voltage, low-cost, earth-abundant, and nontoxic elementals [16-19]. Due to its potential for use in optical parametric oscillators and up converters, in the present technical context, $CdSnP_2$ has several practical applications [20-22]. Using ZnSe as a buffer layer, $CdSnP_2$ thin-film solar cells reach their maximum efficiency of 15.15 percent [23]. Substantial absorptions and high conductivities have been observed in the ultraviolet range for $CdSnP_2$ compounds [24]. A 1.22 eV is the gap value of the direct-gap semiconductor $CdSiP_2$ at its Γ-point [25], He et al. [26] reported that in $CdSiP_2$, the pseudo-direct gap is 1.66 eV, with a structure mechanically stable. Due to a shortage of appropriate emitting substances for (IR) solid state lasers, nonlinear optical (NLO) crystals are required for frequency conversion in order to achieve the mid-IR spectral range over 3 μm [27]. The highest efficiency (25.7%) is demonstrated by $CdSiP_2$ thin-film solar cells [28].

In this work, we focus on ($ZnSiP_2$, $CdSiP_2$, $ZnSnP_2$, and $CdSnP_2$) materials and display findings from density functional theory-based first principles computations of their structural, optoelectronic and electronic characteristics. Structure of the Paper as follows: In section 2, the theoretical framework is presented of our study and shows briefly how it is implemented using computational methods; Results and discussion of the properties are given in Section 3. Finally, Section 4 provides a summary and notes.

2. COMPUTATIONAL DETAILS

Calculations are performed in this investigation using the full-potential linearized augmented plane-wave (FP-LAPW) method carry out by the WIEN2k code [29]. The generalized gradient approximation (PBE-GGA) of Perdew-Burke and Ernzerhof [30] are used to perform geometrical relaxation. The relaxed geometry well-aligned with the experimental data [2,35,36]. The Tran-Blaha modified Becke–Johnson (TB-mBJ) potential is also used to determine the band structure and the related properties [31] based on Density Functional Theory (DFT) [32,33]. In FP-LAPW method the unit cell is partitioned into two regions, inside muffin-tin (MT) spheres that are non-overlapping are centered on the atomic locations, and outside MT sphere an interstitial region (IR). In the IR, a plane wave expansion with cut-off R_{MT} K_{max}= 7, where R_{MT} is the smallest radius of the MT spheres and the magnitude of the biggest K vector in the plane wave expansion is given by K_{max}. The biggest vector in the charge density Fourier expansion, G_{max}, has a value of 12 (a.u) $^{-1}$. The valence wave functions within MT spheres are extended up to I_{max} = 10 and l_{max}= 4 for the interstitial region. The chosen MT radii during the self-consistence calculations are Cd, Zn, Si, Sn and P = 2.21. When the system's total energy is stable within 10^{-5} Ryd , the self-consistent calculations are deemed to have converged. The integrals over the irreducible Brillouin zone (IBZ) are performed with 12×12×12 points.

3. RESULTS AND DISCUSSIONS

3.1. Structural properties

The structure of XYP_2 is shown in fig. 1 Ternary compounds XYP_2 (X =Zn, Cd; Y=Si, Sn) tetragonal body-centered crystals (BCT), with space group $I\bar{4}2d$, each unit cell contains eight atoms. The X-group atoms, Y-group atoms, and P atoms occupy the Wyckoff positions: 4a(0.0,0.0,0.0), 4b(0.0,0.0,0.5), and 8d(u,0.25,0.125) respectively, where u represents anion

displacement parameter (internal distortion parameter). The *c/a* ratio indicates the degree of tetrahedral distortion in the structure; due to these distortions, the c-axis in tetragonal unit cells is nearly twice as large as the a-axis, and chalcopyrite volume being nearly two times that of the zinc blende structure. In the perfect structure, *c/a* =2.0 and *u* =0.25.

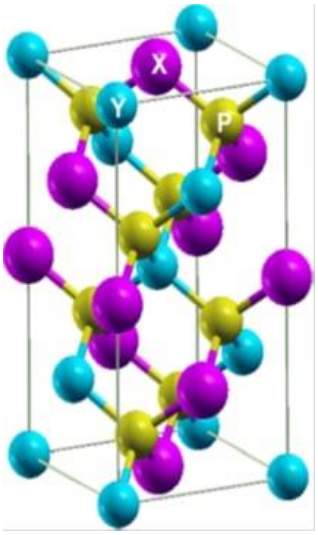

Figure 1 Crystal structure of XYP_2.

3.2. Electronic properties

Band structure and electronic density of states (total and partial) are the focus of this subsection. The atomic configurations are:
Zn^{30}(Ar $3d^{10}$ $4S^2$), Cd^{48}(Kr $4d^{10}$ $5S^2$), Si^{14}(Ne $3S^2$ $3P^2$), Sn^{50}(Kr $4d^{10}$ $5S^2$ $5P^2$), P^{15}(Ne $3S^2$ $3P^3$).
The experimental lattice constants (a, c), and internal parameter (u) along with the calculated lattice constant (a, c) are summarizing in Table 1.

Table 1 Lattice constant (a, c), and internal parameter u.

Compounds		a (Å)	c (Å)	*u*
$ZnSiP_2$	This work	5.396	10.430	
	Experimental	5.399[b]	10.435[b]	0.269[b]
	Calculated	5.405[a]	10.505[a]	0.264[a]
$ZnSnP_2$	This work	5.649	11.301	
	Experimental	5.651[c]	11.302[c]	0.24[c]
	Calculated	5.650[a]	11.300[a]	0.25[a]
$CdSiP_2$	This work	5.677	10.427	
	Experimental	5.680±0.001[f]	10.431±0.003[f]	0.292[f]
	Calculated	5.576[g]	10.415[g]	
$CdSnP_2$	This work	5.898	11.510	
	Experimental	5.901±0.001[e]	11.512±0.002[e]	0.265[e]
	Calculated	6.063[d]	11.604[d]	0.273[d]

[a]Ref. [19] , [b]Ref.[35], [c]Ref. [36], [d]Ref.[34], [e]Ref. [2], [f]Ref. [35], [g]Ref. [52].

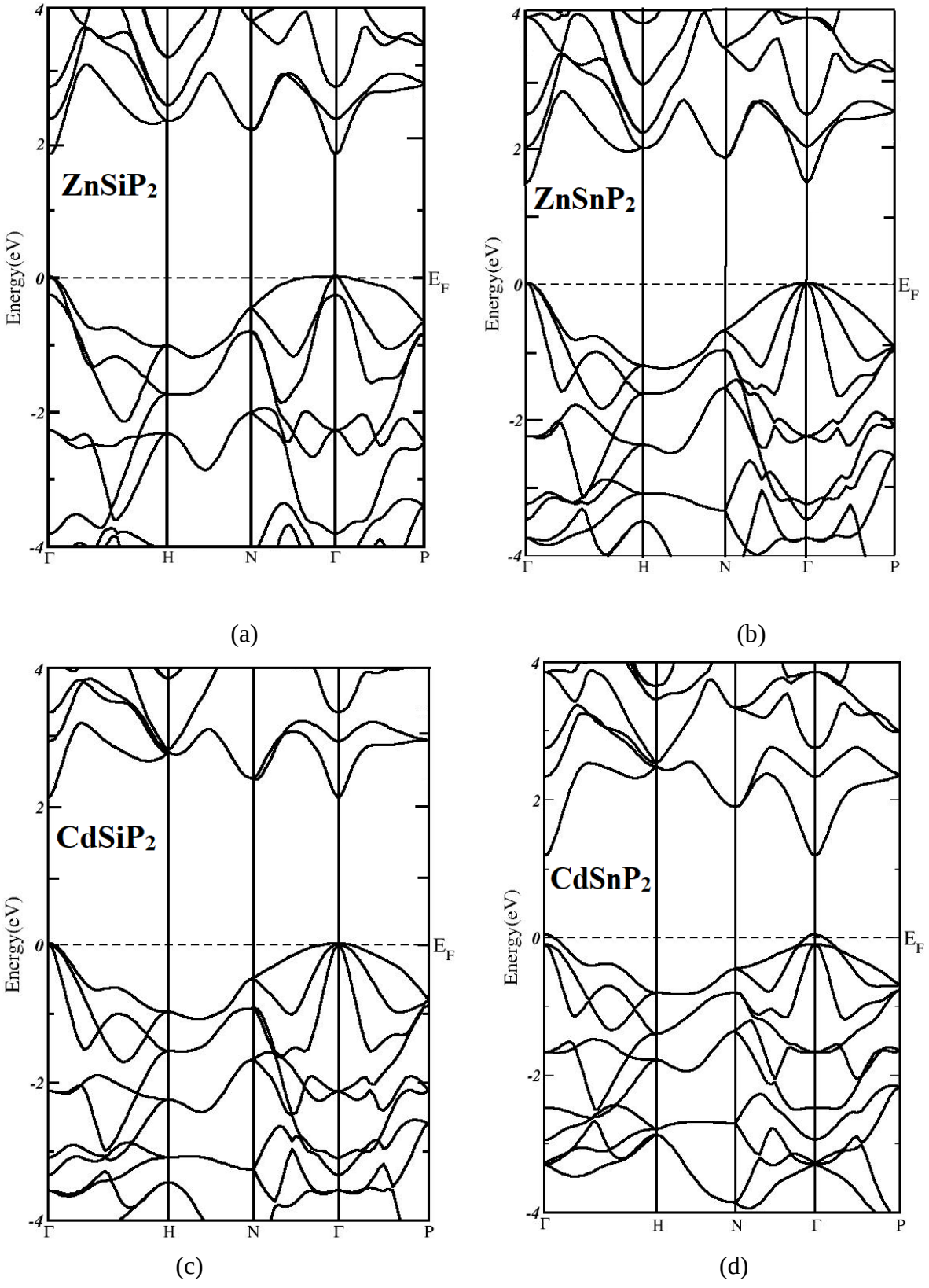

Figure 2 Calculated band structure (a) $ZnSiP_2$, (b) $ZnSnP_2$, (c) $CdSiP_2$ and (d) $CdSnP_2$.

The calculated band structures of XYP_2 are presented in Fig. 2 along the high-symmetry BZ directions. Based on electronic band structures calculations, these compounds are the semiconductor. The maximum of the valence band (VBM) is chosen to concur with the zero energy. The band structures of these compounds differ slightly in details. In all cases, the (VBM) and the minimum of the conduction band (CBM) are located at Γ-point resulting in a

direct energy gap in close agreement with earlier findings [13, 37, 38] for $ZnSnP_2$ and $CdSnP_2$ and $ZnSiP_2$ [15, 19, 42]. While the previous results reported that the $CdSiP_2$ possess an indirect gap [39] and pseudo-direct gap [40-41]. We would like to mention here the previous result reported that the $ZnSiP_2$ have pseudo-direct gap [43]. Table 2 shows the obtained values of the energy bandgaps of XYP_2 compounds, as well as earlier experimental and theoretical data.

Table 2 Calculated bandgaps in (eV) with other previous theoretical and experimental gaps.

Compounds	this work	Experimental	Theoretical
$ZnSiP_2$	1.98 [a]	1.0[b], 2.082[e]	1.32[c] , 1.98[g] , 2.12[f]
$ZnSnP_2$	1.60[a]	1.683[k] , 1.2[d]	1.23[c] , 1.48[g] ,1.58[f]
$CdSiP_2$	2.10[a]	2.2_2.45[g]	2.05[g] ,1.10[i], 1.75[f]
$CdSnP_2$	1.15 [a]	1.17[g]	0.753[h] , 1.05[g], 1.32[f]

[a]This work, [b]Ref. [15], [c]Ref. [19], [d]Ref. [36], [e]Ref. [44], [f]Ref. [20], [g]Ref. [13], [h]Ref[34], [i]Ref[40], [k]Ref. [51].

The decrease in the gap can be attributed due to the reality that the CB's shift towards Fermi energy when on the move from Si to Sn.

3.2.1. Total and Partial Density of States

The total and partial density of states (T/PDOS) for the four II-IV-V_2 type semiconductors are shown in Fig. 3 and Fig. 4 respectively.

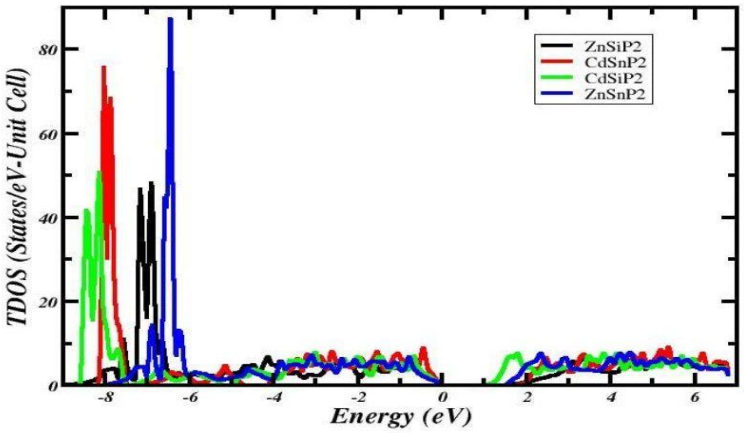

Figure 3 Total density of states (TDOS) for XYP_2.

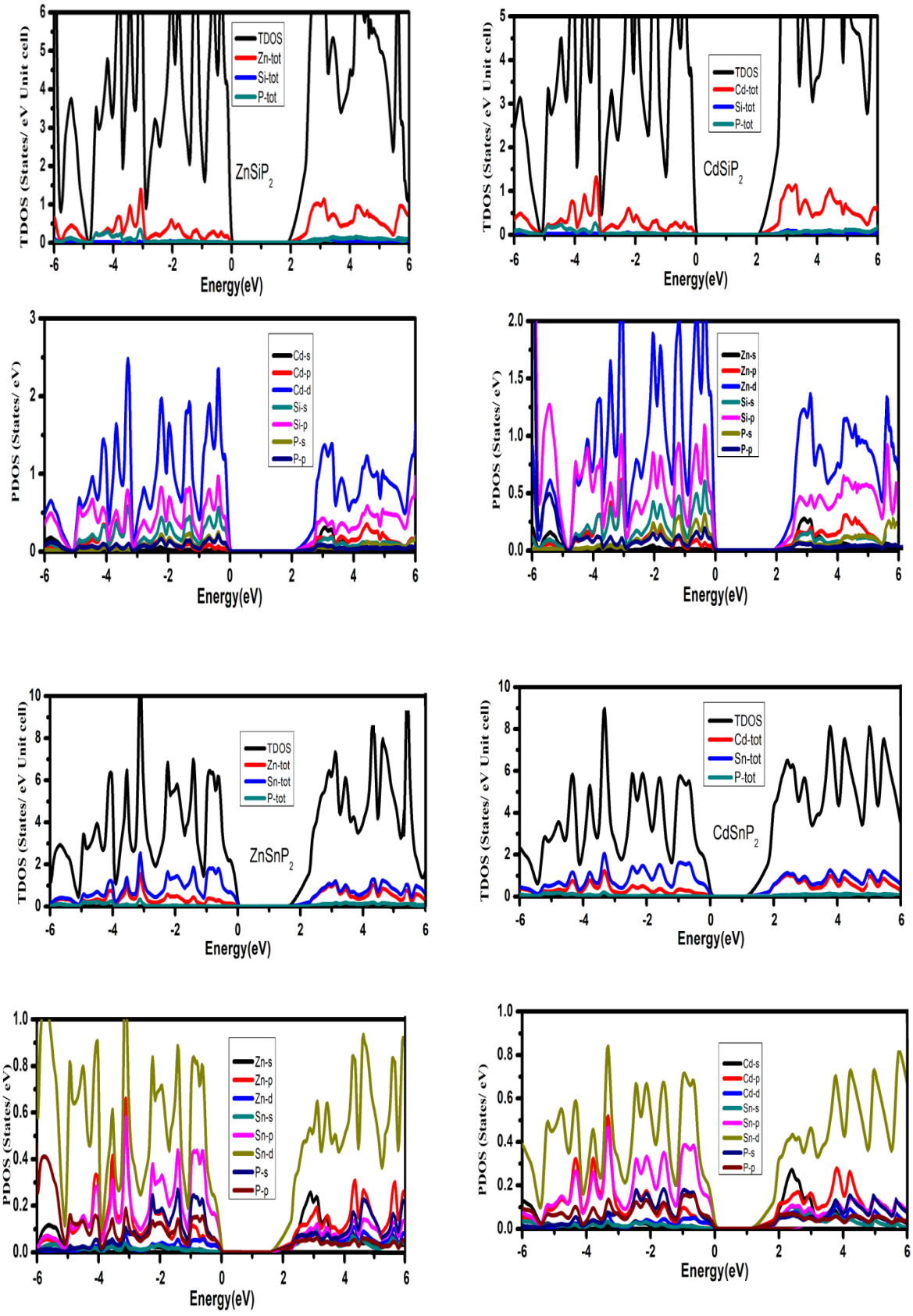

Figure 4 Total and Partial Density of States for XYP_2.

The nature of the TDOS for $ZnSiP_2$ and $CdSiP_2$ are very identical, and the same case for the $ZnSnP_2$ and $CdSnP_2$. In the PDOS, we note that the $ZnSnP_2$ and $CdSnP_2$ are dominated by the contribution of (Sn-d) states in the valence (VB) and conduction (CB) bands, while the $ZnSiP_2$ and $CdSiP_2$ are dominated by the contribution of (Zn/Cd-d) states in the VB and CB, respectively. Fig. 4.(a, b) show that the DOS of $ZnSiP_2$ and $CdSiP_2$ can be partitioned into three notable regions in the VB, the first region in the energy range (-6 to -5 eV) is dominated by the contribution of essentially (Si-p), (Zn-d, P-p), and(Cd-d, Si-p) states, respectively. The second region (-5.4 to -3 eV) it is dominated by the contribution of essentially (Zn/Cd-d, Si-p) with a small mixed contribution of (Si-s, Zn-p, P-p) states for $ZnSiP_2$, the latter region in VBM extend from -3 to Fermi level is formed with significant contributions of (Zn/Cd-d) with small mixed contribution (Si-p,s, P-s), with less (P-p, Zn/Cd-p) states. The CB, consists fundamentally of a mixture of states of type (Zn/Cd-d, p), (Si-p), with less contribution of (Si-s)(Zn/Cd-s) states in the minimum C.B.

Fig. 4.(c, d) show that the electronic DOS of the $ZnSnP_2$ and $CdSnP_2$ can be divided into three notable regions in the VB, the first region in the energy range (from -6 to -5eV) is dominated by the contribution of essentially (Sn-d, P-p), and small mixed contribution of (Zn/Cd-s, Sn-p), and less of (Sn-s) states. The second area is situated between (-5.4 and -3 eV) it is dominated by the contribution of essentially (Sn-d) with a small mixed contribution of (Zn/Cd-p, Sn-p,s, P-p,s) states. The latter region in VBM extend from -3 to Fermi level is formed with significant contributions of (Sn-d) with small mixed contribution (Sn-p, P-s), with less (P-p, Zn-p, Cd-s) states. The CB, consists fundamentally of a mixture of states of type (Sn-d), with small contribution of (Zn/Cd-p, d)(Sn-p, s) (P-p, s), and less of (Zn/Cd-s) states in the minimum CB.

3.3. Optical properties

Optical properties of XYP_2 chalcopyrite can be described by the dielectric function of the semiconductor which obtain from the Ehrenreich and Cohen's equation: $\varepsilon(\omega)= \varepsilon_1(\omega)+ i\varepsilon_2(\omega)$[45], where $\varepsilon_1(\omega)$ is the real part of the dielectric function follows the Kramer and Kroning relations, and $\varepsilon_2(\omega)$ is the imaginary part, and it is the essential factor in the optical properties of matter [46-47]. The dielectric function for $ZnYP_2$(Y=Si, Sn) and $CdYP_2$(Y= Si, Sn) with chalcopyrite structures and space group $I\bar{4}2d$ have only two major optical components. These are $\varepsilon_x(\omega)$ and $\varepsilon_z(\omega)$. Which are plotted for the electrical field vector for ordinary polarization spectra along direction *x* (E⊥c-axis) and $\varepsilon_z(\omega)$ corresponding to the extraordinary polarization along the direction of *z* (E//c-axis). Fig. 5. explain the real and imaginary parts of the electronic dielectric function $\varepsilon(\omega)$ spectrum for a radiation ranging up to 14 eV.

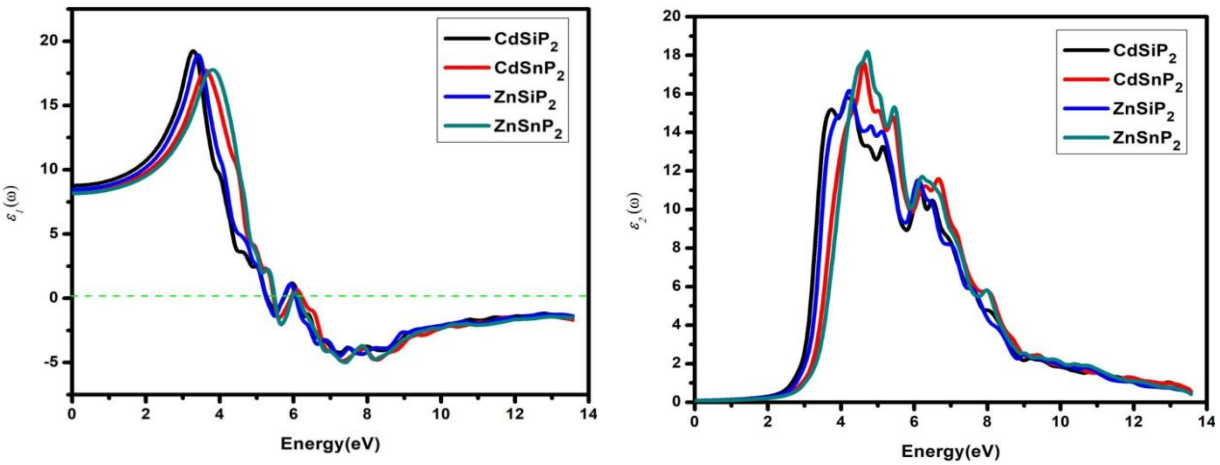

(a) (b)

Figure 5 The calculated (a) real $\varepsilon_1(\omega)$ and (b) imaginary $\varepsilon_2(\omega)$ parts of complex dielectric constant for XYP_2.

The main peaks of $\varepsilon_1(\omega)$ is mainly generated by the transition of electrons from the VBM to the CBM, occur at 3.306, 3.192, 3.724, and 3.496 eV for $ZnSiP_2$, $CdSiP_2$, $ZnSnP_2$, and $CdSnP_2$, respectively. One can obviously see that the $\varepsilon_1(\omega)$ vanishes at the energy values 5.11, 5.11, 5.32, and 5.32eV for $ZnSiP_2$, $CdSiP_2$, $ZnSnP_2$, and $CdSnP_2$, respectively, and all $\varepsilon_1(\omega)$ of XYP_2 becomes negative and reach their minima at around 6.99, 6.99, 7.204, and 7.07 eV for $ZnSiP_2$, $CdSiP_2$, $ZnSnP_2$, and $CdSnP_2$, respectively. Then, at high energy, the spectrum of $\varepsilon_1(\omega)$ progressively increases to zero. For $ZnSiP_2$, $CdSiP_2$, $ZnSnP_2$, and $CdSnP_2$ respectively, the static dielectric constants $\varepsilon_1(0)$ found to be around 8.528, 8.84, 8.216, and 8.44 eV in all directions. Fig. 5. (b) illustrates the imaginary (absorptive) parts $\varepsilon_2(\omega)$, the first critical point (start of absorption) is happening at the energy of 1.824, 1.672, 2.218, and 1.938 eV for $ZnSiP_2$, $CdSiP_2$, $ZnSnP_2$, and $CdSnP_2$, respectively, identical to the main optical energy gap, "Fundamental absorption edges" [48] corresponds to the direct optical (interband) transition between the $V.B_{max}$ and $C.B_{min}$. Then the $\varepsilon_2(\omega)$ curve increases rapidly because the number of points subscribes to $\varepsilon_2(\omega)$ increases sharply. The major peaks occur at about 4.096, 3.99, 4.522, and 4.446 eV for $ZnSiP_2$, $CdSiP_2$, $ZnSnP_2$, and $CdSnP_2$, respectively.

The other optical properties including, absorption coefficient $\alpha(\omega)$, reflectivity $R(\omega)$, extinction coefficient $k(\omega)$, refractive index $n(\omega)$, energy loss function $L(\omega)n$[49,50] can be obtain from the $\varepsilon_1(\omega)$ and $\varepsilon_2(\omega)$. Fig. 6 displays the absorption coefficient $\alpha(\omega)$ for $ZnYP_2$(Y=Si, Sn) and $CdYP_2$(Y= Si, Sn). The $\alpha(\omega)$ is a quantity that describes how much light of electromagnetic wave loses when it travels through a material of a given thickness. From the absorption spectrum, the absorption edges of 2.66, 2.5, 2.812, and 2.738 eV for $ZnSiP_2$, $CdSiP_2$, $ZnSnP_2$, and $CdSnP_2$, respectively. The $\alpha(\omega)$ increases when the photon energy exceeds the value at the absorption edge then it reduced at the high-energy range. The main peaks is located at about ~ 6.15-8.7 eV for XYP_2 compounds in the UV region. In XYP_2, $\alpha(\omega)$ marginally decreases when Zn replaced by Cd and Si by Sn. In close proximity to the major peaks, these compounds show high absorption over a wide energy range and they are well suited for use in solar cell absorbers. The $R(\omega)$ of XYP_2 are displays in Fig. 7. The static value of reflectivity R(0) is 0.237, 0.24, 0.23, and 0.23 for $ZnSiP_2$, $CdSiP_2$, $ZnSnP_2$, and $CdSnP_2$, respectively. First peak occurs at energy about ~3.5-4.8 eV. The maximum reflectivity $R(\omega)$ of XYP_2 lie in the energy range of 8–9 eV at about 0.61-0.628. The calculated extinction coefficient $k(\omega)$ shows in Fig. 8. From $k(\omega)$ spectra the absorption edge occurs at about 1.9, 1.77, 2.06, and 2 eV for $ZnSiP_2$, $CdSiP_2$, $ZnSnP_2$, and $CdSnP_2$

respectively, one can see as photon energy increase, k(ω) decreases. In Fig. 9 the complex refractive index represented by the equation $n\tilde{}\ (\omega) = n(\omega) + ik\ (\omega)$ [24], the refraction and absorption occur when light waves travel through substances. Where $n(\omega)$ is the ordinary refractive index, and $k(\omega)$ is the extinction index, which illustrates the energy photons lose when traveling through an optical medium. The static refractive indexes $n(0)$ are 2.905, 2.95, 2.836, and 2.85 for $ZnSiP_2$, $CdSiP_2$, $ZnSnP_2$, and $CdSnP_2$, respectively. The refractive index $n(\omega)$ peaks reach a maximum value in the ultraviolet (UV-A) zone is about 4.48, 4.48, 4.33, and 4.296 for $ZnSiP_2$, $CdSiP_2$, $ZnSnP_2$, and $CdSnP_2$, respectively at a range energy about 3.34-3.8 eV. Finally, Fig. 10 shows the electron energy-loss function $L(\omega)$, it means there is an electron energy loses when moving through a material. The maximum value of $L(\omega)$ for XYP_2 is located at 13 eV.

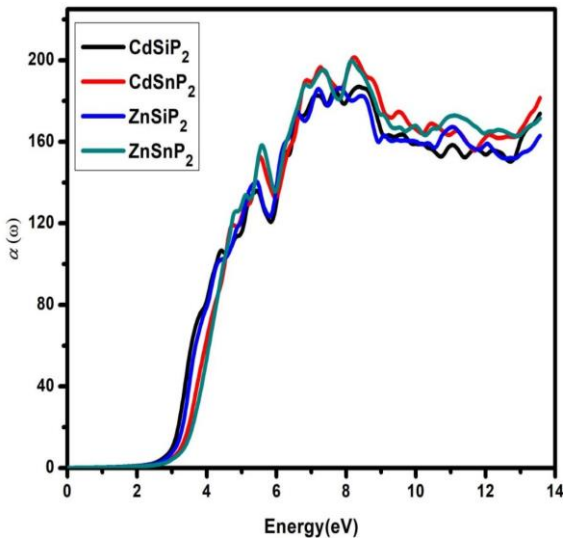

Figure 6 The calculated absorption coefficient α(ω) $10^4 cm^{-1}$.

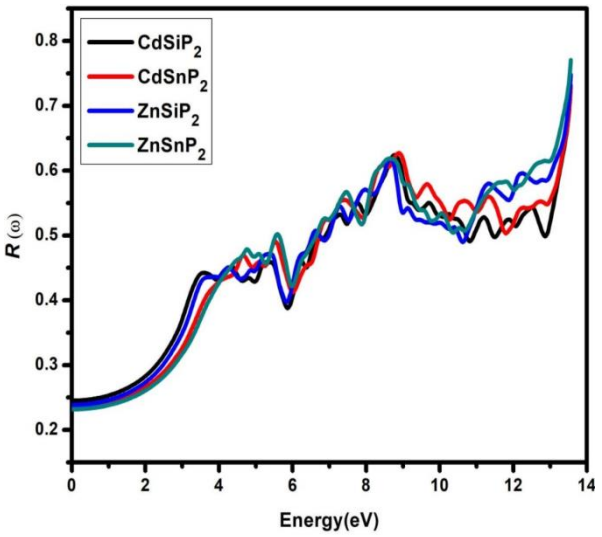

Figure 7 The calculated reflectivity (R (x)).

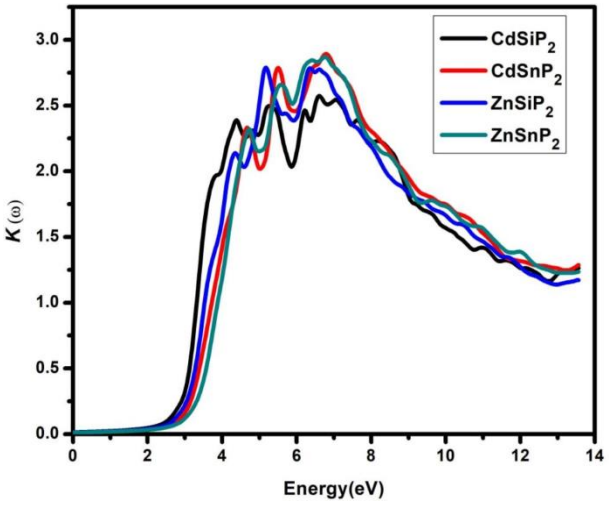

Figure 8 The calculated extinction coefficient.

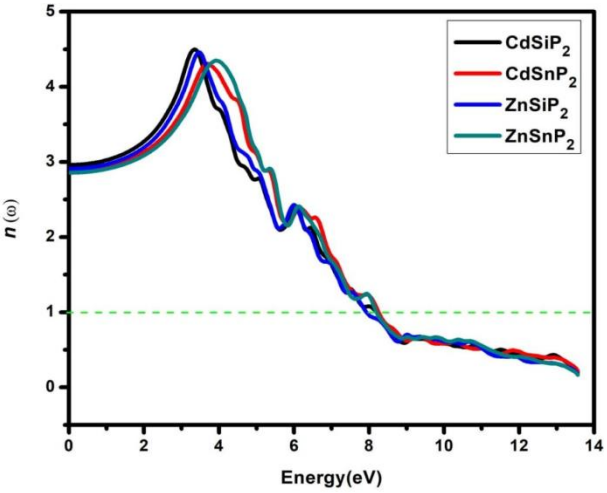

Figure 9 The calculated refractive index coefficient.

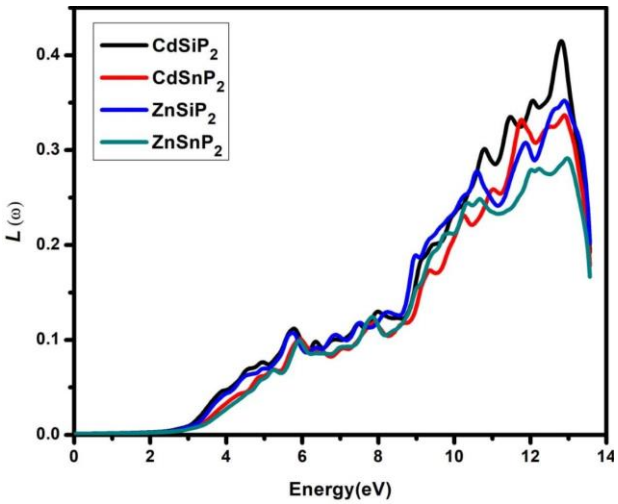

Figure 10 The energy loss spectrum.

4. CONCLUSIONS

The structural, optical, and electronic characteristics of chalcopyrite's XYZ_2 (X= Zn, Cd ; Y= Si, Sn ; Z=P) semiconductors with space group $I\bar{4}2d$ are calculated within DFT. The (PBE-GGA) is used to perform geometrical relaxation and the (TB-mBJ) potential is used to determine the ground state properties. By substituting Si for Sn in XYP_2, the band gap values decrease. Zn and Cd's (d-state) considerable contribution to the density of states in $XSiP_2$, in the $XSnP_2$, Sn-d states are predominant. The calculated partial density of states shows there is a significant degree of hybridization between the states. XYP_2 is a promising material for photonic and optoelectronic devices due to its strong UV reflectance.

References

[1] M. C. Ohmer and R. Pandey, MRS Bulletin 23 (1998) 1622
[2] J. L. Shay, and J. H. Wernick, Ternary Chalcopyrite Semi-conductors: Growth, Electronic Properties and Applications, Pergamon Press, Oxford, (1975)
[3] Kazmerski L L, NuovoCimento 20 (1983) 2013
[4] T. Yokoyama, F. Oba, A. Seko, H. Hayashi, Y. Nose, I. Tanaka., Applied Physics Express 6 (2013) 061201
[5] C. Yan and D. Xue, Funct. Mater. Lett. 1 (2008) 37
[6] J. L. Shay, K. J. Bachmann, E. Buehler, J. H. Wernick., Applied Physics Letters 23 (1973) 226
[7] U. Rau and H. W. Schock, Appl. Phys. A 69 (1999) 131
[8] B. J. Stanbery, Crit. Rev. Solid State Mater. Sci. 27 (2002) 73
[9] J. Kessler, J. Wennerberg, M. Bodegard, L. Stolt, Sol. Energy Mater.Sol. Cells 75 (2003) 35
[10] G. C. Bhar, Jpn. J. Appl. Phys. Suppl. 653 (1993) 32
[11] Z. Zhang, D. T. Reid, S. C. Kumar, M. E.-Zadeh, P. G. Schunemann, K. T. Zawilski, C. R. Howle. Optics Letters, 38 (2013) 5110
[12] W. Feng, D. Xiao, J. Ding, Y. Yao, Phys. Rev. Lett. 106 (2011) 016402
[13] V.L. Shaposhnikov, A.V. Krivosheeva, V.E. Borisenko, J.L. Lazzari, F.A. Avitaya, Phys. Rev. B 85 (2012) 205201
[14] D. O. Scanlon, & A. Walsh, Appl. Phys. Lett. 100 (2012) 251911
[15] J. L. Shay, B. Tell, E. Buehler, & J. H. Wernick, Phys. Rev. Lett. 30 (1973) 983
[16] Martinez, A. D. et al. Energy Environ. Sci. 9 (2016) 1031

[17] Martinez, A. D., Fioretti, A. N., Toberer, E. S. & Tamboli, A. C. J. Mater. Chem. A 5 (2017) 11418
[18] Martinez, A. D. et al. J. Mater. Chem. C 6 (2018) 2696
[19] Liu, H. et al. Mater. Res. Express 5 (2018) 126303
[20] Verma, A. S. Physica Status Solidi (b), 246 (2009) 192
[21] C. H. L. Goodman, Semiconductor Science and Technology 6 (1991) 725
[22] V. Petrov, Progress in Quantum Electronics 44 (2015) 654
[23] Gautam, R., Singh, P., Sharma, S., Kumari, S., & Verma, A. S. Superlattices and Microstructures 85 (2015) 859
[24] Sibghat ullah, G. Murtaza, R. Khenata, A. H. Reshak, S. S. Hayat, S. Bin Omran. Physica B 441 (2014) 94
[25] Lv, Z.-L., Cheng, Y., Chen, X.-R., & Ji, G.-F. Computational Materials Science 77 (2013) 114
[26] He, Z., Zhao, B., Zhu, S., Chen, B., Hou, H., Yu, Y., & Xie, L. Computational Materials Science 72 (2013) 26
[27] V. Petrov, F. Noack, I. Tunchev, P. Schunemann, K. Zawilski, Proc. SPIE 21 (2009) 7197
[28] Verma, A. S., Gautam, R., Singh, P., Sharma, S., Kumari, S. Materials Science and Engineering B 205 (2016) 18
[29] P. Blaha, K. Schwarz, G.K.H. Madsen, D. Kvasnicka, J. Luitz, Technisch Universitat, Wien, Austria, ISBN 3-9501031-1-2, (2001)
[30] J.P. Perdew, K. Burke, M. Ernzerhof, Phys. Rev. Letts. 77 (1996) 3865
[31] F. Tran, P. Blaha, Phys. Rev. Lett. 102 (2009) 226401
[32] P. Hohenberg, W. Kohn, Phys. Rev. B 136 (1964) 864
[33] W. Kohn, L. J. Sham, Phys. Rev. A 140 (1965) 1133
[34] Hu, J., Shi, L., Qin, Y., Jin, F., Duan, Y., Qiu, L., & Chen, L. Materials Science in Semiconductor Processing 35 (2015) 149
[35] Abrahams, S. C., & Bernstein, J. L. The Journal of Chemical Physics, 55 (1971) 796
[36] Rubenstein, M., Ure, R. W. Journal of Physics and Chemistry of Solids 29 (1968) 551
[37] Chiker, F., Abbar, B., Aourag, H., Tadjer, A., Bresson, S., Khelifa, B., Mathieu, C. Chemical Physics 298 (1968) 135
[38] Sahin, S., Ciftci, Y. O., Colakoglu, K., Korozlu, N. Journal of Alloys and Compounds 529 (2012) 1
[39] Isomura, S., & Masumoto, K. Physica Status Solidi (a) 6 (1971) K139
[40] Chiker, F., Abbar, B., Tadjer, A., Aourag, H., Khelifa, B. Materials Science and Engineering B 98 (2003) 81
[41] Chiker, F., Abbar, B., Tadjer, A., Bresson, S., Khelifa, B., & Mathieu, C. Physica B: Condensed Matter 349 (2004) 181
[42] Sreeparvathy, P. C., Kanchana, V., & Vaitheeswaran, G. Journal of Applied Physics 119 (2016) 085701
[43] J. E. Jaffe, and A. Zunger, Physical Review B 30 (1984) 741
[44] Humphreys, R. G., & Pamplin, B. R. Le Journal de Physique Colloques 36 (1975) C3
[45] K. Bougherara, F. Litimein, R. Khenata, E. Uçgun, H.Y. Ocak, S¸. Ugur, G.Ugur, A.H. Reshak, F. Soyalp, S. Bin-Omran, Sci. Adv. Mater. 5 (2013) 97
[46] M. Born, K. Huang, Dynamical Theory of Crystal Lattices, oxford University Press, Oxford, (1954)
[47] Fox, M. "Optical properties of solids; Second ed."; Oxford University Press: New York, (2010)
[48] S. Sahin, Y.O. Ciftci, K. Colakoglu, N. Korozlu, J. Alloy. Comp. 529 (2012) 1
[49] Y. Shen, Z. Zhou, J. Appl. Phys. 103 (2008) 074113

[50] Gani, A., Cheref, O., Ghezali, M., Rabah, M., Reshak, A. H., Djaballah, Y., Belasri, A. Chinese Journal of Physics 47 (2020) 547
[51] St-jean P, Seryogin G.A., Francoeur S, Appl. Phys. Lett. 96 (2010) 231913
[52] Hou, H. J., Zhu, H. J., Xu, J., Zhang, S. R., Xie, L. H. Brazilian Journal of Physics 46 (2016) 628